Bioinspired dual mode temporal communication via digital programmable phase change materials

Shihong Deng
  State Key Laboratory of Chemical Engineering, College of Chemical and Biological Engineering, Zhejiang University

Limei Huang
  State Key Laboratory of Chemical Engineering, College of Chemical and Biological Engineering, Zhejiang University

Jingjun Wu
  Zhejiang Unviersity

Pengju Pan
  State Key Laboratory of Chemical Engineering, College of Chemical and Biological Engineering, Zhejiang University

Qian Zhao (✉ qianzhao@zju.edu.cn)
  State Key Laboratory of Chemical Engineering, College of Chemical and Biological Engineering, Zhejiang University   https://orcid.org/0000-0002-6931-9859

Tao Xie
  Zhejiang University   https://orcid.org/0000-0003-0222-9717

Article

Bioinspired dual mode temporal communication via digital programmable phase change materials

Shihong Deng[1]†, Limei Huang[1]†, Jingjun Wu[1,2], Pengju Pan[1], Qian Zhao[1,2]*, Tao Xie[1,2]

[1]State Key Laboratory of Chemical Engineering, College of Chemical and Biological Engineering, Zhejiang University, Hangzhou 310027, China.

[2]ZJU-Hangzhou Global Scientific and Technological Innovation Center, Hangzhou 311215, China.

*Correspondence and requests for materials should be addressed to Q.Z. (e-mail: qianzhao@zju.edu.cn)

†These authors contributed equally to this work.

Abstract: Switchable optical properties are essential for numerous technologies including communication, anticounterfeiting, camouflage, and imaging/sensing. Typically, the switching is enabled by applying external stimulation such as UV light for fluorescence detection. In contrast, ground squirrels utilize spontaneous live infrared emission for fencing off predators as a unique way of communication. Inspired by this, we demonstrate live evolution of both optical and thermal images for temporal communication in which time is the encoded information. Our system is based on a digital light cured polymeric phase change material for which the crystallization kinetics can be controlled in a pixelated manner. Consequently, live evolution in optical transparency during the crystallization process enables temporal optical communication. Additionally, by harnessing the dynamic evolution of the thermal enthalpy, multiple sets of time specific information can be reversibly retrieved as self-evolving infrared thermal images. The versatility of our dual mode temporal system expands the scope for secured communication, with potential implications for many other areas.

Being adaptive to the surrounding environment is crucial for animals surviving in the wild. Amongst numerous examples, cephalopods achieve camouflage via adaptive color switching whereas chameleons shift colors to express their emotion[1-2]. Inspired by these biological systems, many artificial materials capable of switching optical properties have been invented. Their underlying mechanisms are diverse, including notably photo-luminescence[3-6], photonic crystals[7-9],and thermo-/electro-/mechano-chromism[10-13]. This has led to many technological innovations such as biomedical sensing/imaging[4-5], anticounterfeiting[3], displays[11-12], and smart windows[14-15].

While humans and most animals are mostly sensitive to optical changes, some creatures such as mosquitos and vampire bats rely on infrared emission for seeing in the dark[16-17]. Infrared emission is strongly associated with temperature and its detection/manipulation is uniquely important for medical sensing and camouflage. For instance, infrared based thermography allows quick detection of fever. For camouflage, the goal is to conceal the infrared emission[18-19]. Active manipulation of infrared patterns is possible[20] but self-evolving pattern switching is not known. Intriguingly, certain animals utilize infrared emission as an active mechanism for communication. Specifically, rattlesnakes rely on their infrared sensitive pit organs for detecting preys in the dark[21]. To threaten off rattlesnakes, ground squirrels emit strong and deceptive infrared tail flagging signals by increasing blood flow to the tails[22]. Inspired by the active thermoregulation of ground squirrels and the intended functions, we report hereafter our effort in designing a digitally programmable polymeric phase change material as a self-evolving communication platform. Its most notable feature is that it allows writing multiple temporal thermal information that can only be retrieved at specific time domains encoded into the material system. In addition, since the polymeric phase change material operates via melt/crystallization, the associated change in optical transparency simultaneously permits temporal

optical communication. We show that the dual modes (thermal and optical) work in a synergetic way to not only broaden the working conditions but also enhance the level of security.

Main text

Our system/device is created by photo-curing of a preheated liquid precursor (70 °C) consisting of a crystallizable monomer (stearyl acrylate), a crosslinker (1,6-hexanediol diacrylate), and a photo-initiator (Fig. 1a). A commercial projector generates a digital light pattern to trigger the curing reaction[23]. The digital light exposure allows spatio-temporal control of the polymer network formation, with notable simplicity and versatility beyond other methods that can program polymers in a pixelated manner[24-26]. Here, longer light exposure (region 1 in Fig. 1b) results in a higher crosslink density with less unreacted crystallizable monomer. In contrast, region 2 in Fig. 1b receives shorter light exposure, leading to a network with lower crosslink density with more unreacted crystallizable monomer. Upon cooling after the curing, the two regions should show distinctive crystallization behaviors due to their different network structures. In the time evolution of the cooling induced crystallization process, one possible scenario is that region 1 crystallizes first since the higher crosslinking may result in a high crystallization temperature due to the more established network. Upon further cooling to the full/equilibrium crystallization states, the situation reverses. The region 2 should reach a higher equilibrium crystallinity due to the less constraint in the molecular mobility in a lower crosslinked network. The different trends in the crystallization order and equilibrium crystallinity should lead to corresponding change in optical transmission since the crystallized regions would block light transmission.

Figure 1c confirms the above hypotheses. A thin film sample produced with a cup-shaped light

pattern appears transparent in its melt states at 70 °C. Upon cooling (to 20 °C unless otherwise noted), the regions corresponding to a longer light exposure of 16 s becomes opaque first. Upon further cooling, the regions corresponding to a shorter light exposure of 8 s appear more opaque at the equilibrium crystallization state. The overall result is that the "cup" shape evolves with time into a "face" shape, as captured in Supplementary Movie S1. To reflect the versatility of our fabrication process, a checkerboard pattern can be created following an identical fabrication process except the digital file. This pattern also shows similar time evolving optical changes. The optical evolution is fully reversible by simply heating the devices back to the melt states at 70 °C. This reversibility is applicable to all the other demonstrations shown hereafter.

For quantitative understanding of the above phenomena, we fabricate several films with various light curing times labelled as PSA-X with "X" being the curing time in seconds. Fig. S1 shows the curing kinetics and Fig. S2 confirms that the gel content increases with time. Fig. 2a shows the time evolution of their visible light transmittance upon cooling. The comparison between PSA-16 and PSA-8 clearly shows that the light transmission of the former reduces at a faster pace, but reaches an equilibrium value higher than that of the latter, consistent with the observations in Fig. 1c. This trend is also applicable to PSA-24. For PSA-48, its transmission descends much slower than other samples before reaching a high plateau value around 85%. This suggests its poor tendency toward crystallization as a result of excessive crosslinking.

Figure 2b illustrates the enthalpy evolution during the cooling induced crystallization. The unreacted stearyl acrylate monomer has a main exothermal peak at 27 °C. Two small peaks at 10 and 37 °C are also present due to its polymorphic nature[27]. By comparison, PSA-8 shows a broader exothermic peak at a slightly higher temperature. For the samples of longer curing times, the crystallization

temperature gradually increases whereas the corresponding enthalpy (peak area) follows an opposite trend. This suggests lower crystallinity as the result of longer curing, consistent with the XRD results in Fig. 2c which shows that the diffraction peak broadens with the curing time.

Figure 2d illustrates the equilibrium optical contrast corresponding to various curing time combinations denoted as PSA-X/Y with X and Y being the two curing times. Herein, a fixed curing time of 8 s is used in the opaque regions (the zebras) whereas the background curing time is varied. Compared to PSA-8/16, PSA-8/24 offers a much higher contrast due to the increased background transmission, consistent with Fig. 2a. Although Fig. 2a suggests further increase the background curing time to 48 s should lead to an even better contrast, the reality is the opposite with the image of PSA-8/48 appearing severely blurred. We believe this is because an excessively long curing time of 48 s causes radical diffusion outside the irradiated regions. Guided by the above results, a series of images of high contrast are obtained (Fig. 2e) using the PSA-8/24 combination. We note that the spatial resolution of our system is around 150 μm (Fig. S3), limited largely by the light resolution of the projector which is 100 μm.

The above results set the stage for making programmable time-encrypted devices. Fig. 3a shows two quick response (QR) codes based on PSA-8/24 and PSA-8/12 combinations, respectively. The encoded information is not readable in their transparent melt states. Upon cooling, the PSA-8/24 device becomes scannable at time domains beyond 300 s when the system shows sufficient contrast as the regions approaching full crystallization. By comparison, the information hidden in PSA-8/12 is only retrievable between 100-150 s beyond which the required contrast is lost, which is captured in Supplementary Movie S2. To take this one step further, a temporal QR code film is overlaid on a regular QR code as the background. At the melted state, only the background QR code is scannable

(left figure in Fig. 3B). Upon cooling to 200 s, the overlaying of the two QR codes is such that the device is no longer readable. Upon further cooling to 600 s, the foreground temporal QR code becomes dominant and a new information becomes accessible by scanning. Overall, Fig. 3a and Fig. 3b show that temporal optical information can be encoded for additional security beyond regular QR devices.

We next explore the exothermic nature of the crystallization for infrared based temporal communication. Fig. 3c illustrates that an optically readable pattern is invisible under infrared. It remains infrared unreadable upon heating to its melted state. However, upon cooling at 25 °C, the information becomes readable at 20 s (note: time counting starts from 40 °C). Upon further cooling, the infrared contrast gradually disappears and the information is lost. This intriguing temporal evolution is captured in Movie S3. The above phenomenon arises from the phase change nature of the networks in which the programmable exothermic crystallization in the selected regions temporarily delay the temperature change. Fig. 3d illustrates that an optical pattern becomes undetectable when combined with a complex optical background. Utilizing the phase change principle, however, this pattern can be retrieved as an infrared signal by heating and subsequent cooling, again only at a specific time domain. The comparison of the same device under visible light and infrared camera is shown in Movie S4.

More complex manipulation of temporal infrared information is feasible by employing more than two curing times on a particular set of pattern. Using the combination of three curing times, an optical pattern of a night-blooming epiphyllum is created (Fig. 4a). The dynamic evolution of the infrared pattern upon cooling is captured in Fig. 4a, showing its emergence and disappearance over time. In particular, while the epiphyllum is fully visible at 10 s and 20 s, their infrared contrast

appears distinctively different. The two sets of central petals are clearly distinguishable at 10 s whereas their contrast is lost at 20 s (see Supplementary Movie S5). Taking this concept further, a snake-squirrel combination pattern is fabricated, with both images optically visible (Fig. 4b). Upon melting and subsequent cooling, both the snake and squirrel emerge at 10 s as infrared images. At 40 s, the snake disappears whereas the squirrel remains present, mimicking a scenario in which a ground squirrel scares away a rattlesnake. Both creatures vanish eventually, but the entire evolution cycle can be repeated by heating and cooling.

Discussion

In summary, this work demonstrates the use of digital light curing of a phase change material for programming temporal information. The simplicity in materials and fabrication process is favorable for potential commercial implementation. The use of time as a live dimension increases the amount of stored information and the level of security. The dual operating modes (optical and thermal) further extend the versatility and the temporal information can be naturally monitored without requiring any sophisticated equipment. While this work focuses on temporal communication, we believe that the unexpected benefits illustrated here can inspire advances in many other areas.

Methods

Materials: Stearyl acrylate and 1,6-hexanediol diacrylate were purchased from J&K scientific corporation. Irgacure 819 was obtained from TCI. Prior to their use, the inhibitor in the monomer and crosslinker was removed using an inhibitor remover from Sigma-Aldrich.

Digital light printing: Irgacure 819, 1,6-hexanediol diacrylate, and stearyl acrylate were mixed at a

weight ratio of 1:10:100 and the mixture was vigorously stirred at 70 °C to make a homogenous solution. Digital pattern model files in a stl format were produced using AutoCAD. The light curing reaction cell consisted of two glass slides separated by a silicone spacer (0.5 mm thick). The preheated liquid curing precursor was injected into the reaction cell and a commercial projector (DELL 1609WX) was used for the digital curing.

Measurement of curing kinetics and gel contents: Double bond conversion was measured by a Nicolet 5700 FT-IR spectrometer (Madison, WI) in the Attenuated Total Reflection mode. The conversion was calculated by the decrease of the acrylate characteristic band at 810 cm-1. Films with various curing times were weighed and immersed in n-hexane for 24 hours, then dried in 70 °C oven for 12 hours. Gel contents were calculated as the weight ratios between the dried samples and the original samples.

Material characterization: The light transmission was measured using a handheld transmission meter (model) manufactured by 3M corporation. Differential scanning calorimetry measurements were conducted using a TA Q200 instrument under nitrogen atmosphere and the cooling rate was 1 °C/min. X-Ray diffraction experiments were carried out with a Bruker D8 Advance instrument using Ni-filtered Cu Kα radiation ($\lambda = 0.154$ nm) and the scanning rate was set as 8°/min. The real-time infrared pattern evolution was recorded by a Fotric 237 thermometer with video-capturing capability.

Data availability

The data that support the findings of this study are available from the corresponding

author on reasonable request.

References:

1. Vaia, R. & Baur, J. Adaptive composites. *Science* **319**, 420-421(2008).

2. Teyssier, J., Saenko, S. V., van der Marel, D. & Milinkovitch, M. C. Photonic crystals cause active colour change in chameleons. *Nat. Comm.* **6**, 6368 (2015).

3. Zhao, Y., Zhao, X., Li, M., Li, Z., Peng, H. & Xie, X. Crosstalk-free patterning of cooperative-thermoresponse images by the synergy of the AIEgen with the liquid crystal. *Angew. Chem. Int. Ed.* **59**, 10066-10072 (2020).

4. Wei, P., Zhang, J., Zhao, Z., Chen, Y., He, X., Chen, M., Gong, J., Sung, H. H., Williams, L. D., Lam, J. W. Y. & Tang, B. Multiple yet controllable photoswitching in a single AIEgen system. *J. Am. Chem. Soc.* **140**, 1966-1975 (2018).

5. Zhang, J., Fu, Y., Han, H., Zang, Y., Li, J., He, X., Feringa, B. L. & Tian, H. Remote light-controlled intracellular target recognition by photochromic fluorescent glycoprobes. *Nat. Comm.* **8**. 987 (2017).

6. Tao, S., Lu, S., Geng, Y., Zhu, S., Redfern, S. A. T., Song, Y., Feng, T., Xu, W. & Yang, B. Design of metal-free polymer carbon dots: a new class of room-temperature phosphorescent materials. *Angew. Chem. Int. Ed.* **57**, 2393-2398 (2018).

7. Vatankhah-Varnosfaderani, M., Keith, A. N., Cong, Y., Liang, H., Rosenthal, M., Sztucki, M., Clair, C., Magonov, S., Ivanov, D. A., Dobrynin, A. V. & Sheiko, S. S. Chameleon-like elastomers with molecularly encoded strain-adaptive stiffening and coloration. *Science* **359**, 1509-1513 (2018).

8. Ito, M. M., Gibbons, A. H., Qin, D., Yamamoto, D., Jiang, H., Yamaguchi, D., Tanaka, K. & Sivaniah, E. Structural colour using organized microfibrillation in glassy polymer films. *Nature* **570**, 363-375 (2019).

9. Qin, M., Sun, M., Bai, R., Mao, Y., Qian, X., Sikka, D., Zhao, Y., Qi, H. J., Suo, Z. & He, X. Bioinspired hydrogel interferometer for adaptive coloration and chemical sensing. *Adv. Mater*. **30,** 1800468 (2018).

10. Jin, Y., Lin, Y., Kiani, A., Joshipura, I. D., Ge, M. & Dickey, M. D. Materials tactile logic via innervated soft thermochromic elastomers. *Nat. Comm.* **10**, 4187 (2019).

11. Yu, C., Li, Y., Zhang, X., Malyarchuk, V., Wang, S., Shi, Y., Gao, L., Su, Y., Zhang, Y., Xu, H., Hanlon, R. T., Huang, Y. & Rogers, J. A. Adaptive optoelectronic camouflage systems with designs inspired by cephalopod skins. *Proc. Natl. Acad. Sci. USA*. **111**, 12998-13003 (2014).

12. Wang, C., Hwang, D., Yu, Z., Takei, K., Park, J., Chen, T., Ma, B. & Javey, A. User-interactive electronic skin for instantaneous pressure visualization. *Nat. Mater*. **12**, 899-904 (2013).

13. Lavrenova, A., Balkenende, D. W. R., Sagara, Y., Schrettl, S., Simon, Y. C. & Weder, C. Mechano- and thermoresponsive photoluminescent supramolecular polymer. *J. Am. Chem. Soc.* **139**, 4302-4305 (2017).

14. Kosa, T., Sukhomlinova, L., Su, L., Taheri, B., White, T. J. & Bunning, T. J. Light-induced liquid crystallinity. *Nature* **485**, 347-349 (2012).

15. Kim, H. N., Ge, D., Lee, E. & Yang, S. Multistate and on-demand smart windows. *Adv. Mater.* **30**, 1803847 (2018).

16. van Breugel, F., Riffell, J., Fairhall, A. & Dickinson, M. H. Mosquitoes use vision to associate odor plumes with thermal targets. *Curr. Biol*. **25**, 2123-2129 (2015).

17. Gracheva, E. O., Cordero-Morales, J. F., González-Carcacía, J. A., Ingolia, N. T., Manno, C., Aranguren, C. I., Weissman, J. S. & Julius, D. Ganglion-specific splicing of TRPV1 underlies infrared sensation in vampire bats. *Nature* **476**, 88-91 (2011).

18. Li, M., Liu, D., Cheng, H., Peng, L. & Zu, M. Manipulating metals for adaptive thermal camouflage. *Sci. Adv*. **6**, eaba3494 (2020).

19. Han, T., Bai, X., Thong, J. T. L., Li, B. & Qiu, C. Full control and manipulation of heat signatures: cloaking, camouflage and thermal metamaterials. *Adv. Mater*. **26**, 1731-1734 (2014).

20. Xu, C., Stiubianu, G. T. & Gorodetsky, A. A. Adaptive infrared-reflecting systems inspired by cephalopods. *Science* **359**, 1495-1500 (2018).

21. Gracheva, E. O., Ingolia, N. T., Kelly, Y. M., Cordero-Morales, J. F., Hollopeter, G., Chesler, A. T., Sánchez, E. E., Perez, J. C., Weissman, J. S. & Julius, D. Molecular basis of infrared detection by snakes. *Nature* **464**, 1006-1011 (2010).

22. Rundus, A. S., Owings, D. H., Joshi, S. S., Chinn, E. & Giannini, N. Ground squirrels use an infrared signal to deter rattlesnake predation. *Proc. Natl. Acad. Sci. USA*. **104**, 14372-14376 (2007).

23. Huang, L., Jiang, R., Wu, J., Song, J., Bai, H., Li, B., Zhao, Q. & Xie, T. Ultrafast digital printing toward 4D shape changing materials. *Adv. Mater*. **29**, 1605390 (2017).

24. Kim, J., Hanna, J. A., Byun, M., Santangelo, C. D. & Hayward, R. C. Designing responsive buckled surfaces by halftone gel lithography. *Science* **335**, 1201-1205 (2012).

25. Ware, T. H., McConney, M. E., Wie, J. J., Tondiglia, V. P. & White, T. J. Voxelated liquid crystal elastomers. *Science* **347**, 982-984 (2015).

26. Zhang, G., Peng, W., Wu, J., Zhao, Q. & Xie, T. Digital coding of mechanical stress in a dynamic covalent shape memory polymer network. *Nat. Comm.* **9**, 4002 (2018).

27. Miao, Y., Nie, J. & He, Y. Can chain-reaction polymerization of octadecyl acrylate occur in crystal? *Macromolecules* **51**, 3731-3737 (2018).

Competing interests: The authors declare no competing financial interests.

Reprints and permission information is available online at http://npg.nature.com/ reprintsandpermissions/

Publisher's note: Springer Nature remains neutral with regard to jurisdictional claims in published maps and institutional affiliations.

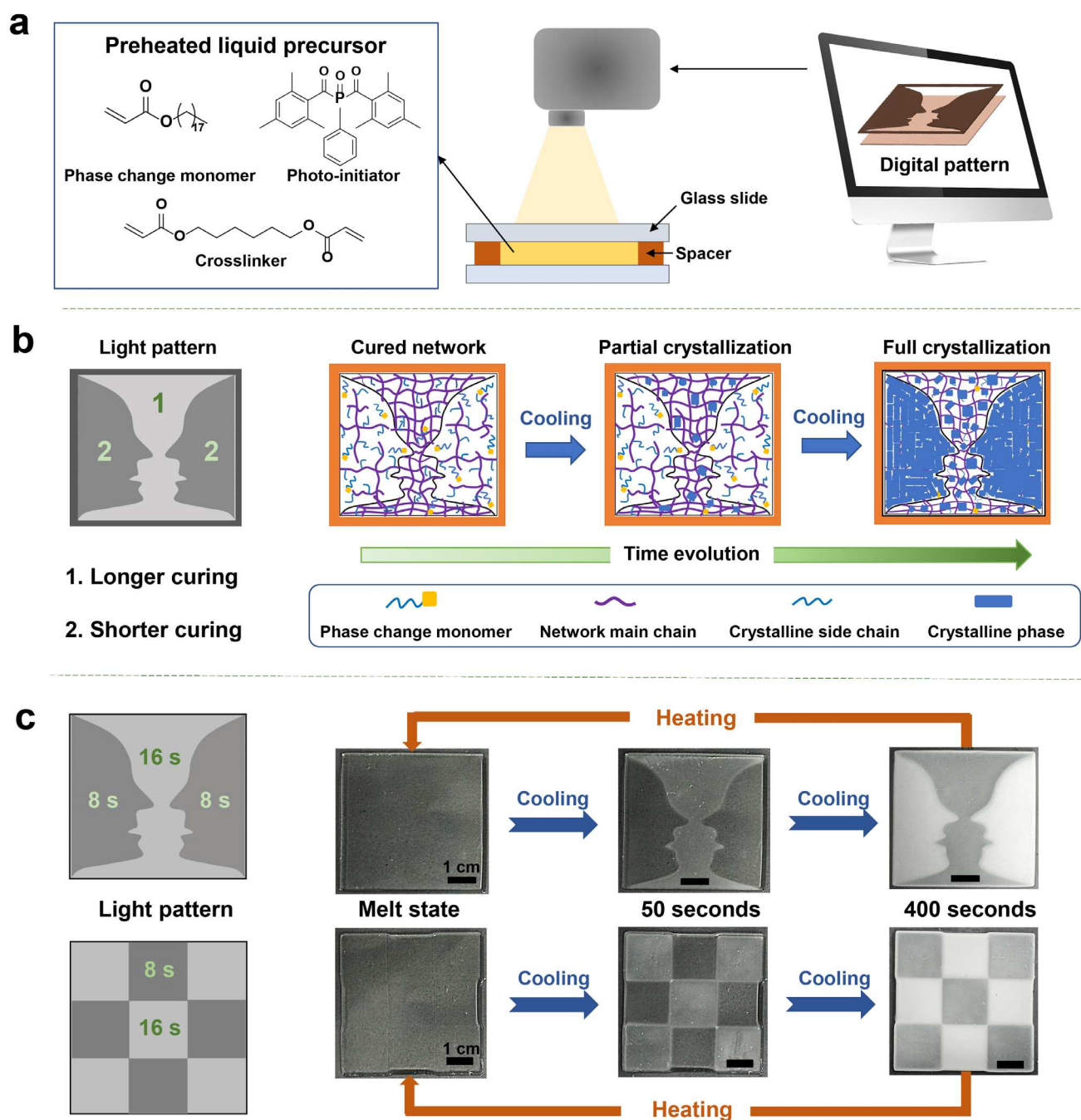**Fig. 1 Materials, fabrication, and operating principle of the digital programmable phase change material**. **a.** Precursors and digital curing setup. **b.** Light controlled network formation and crystallization. **c.** Reversal of the optical contrast for two digital cured patterns.

Fig. 2 Crystallization behaviors of digitally cured phase change material and the optical contrast optimization. a. Time evolution of visible light transmittance upon cooling. **b.** Differential scanning calorimetry (DSC) crystallization curves. **c.** XRD patterns. **d.** Comparison of the optical contrast for the patterned samples with different curing time combinations. **e.** Diverse optical patterns with colored backgrounds obtained with a PSA-8/24 combination.
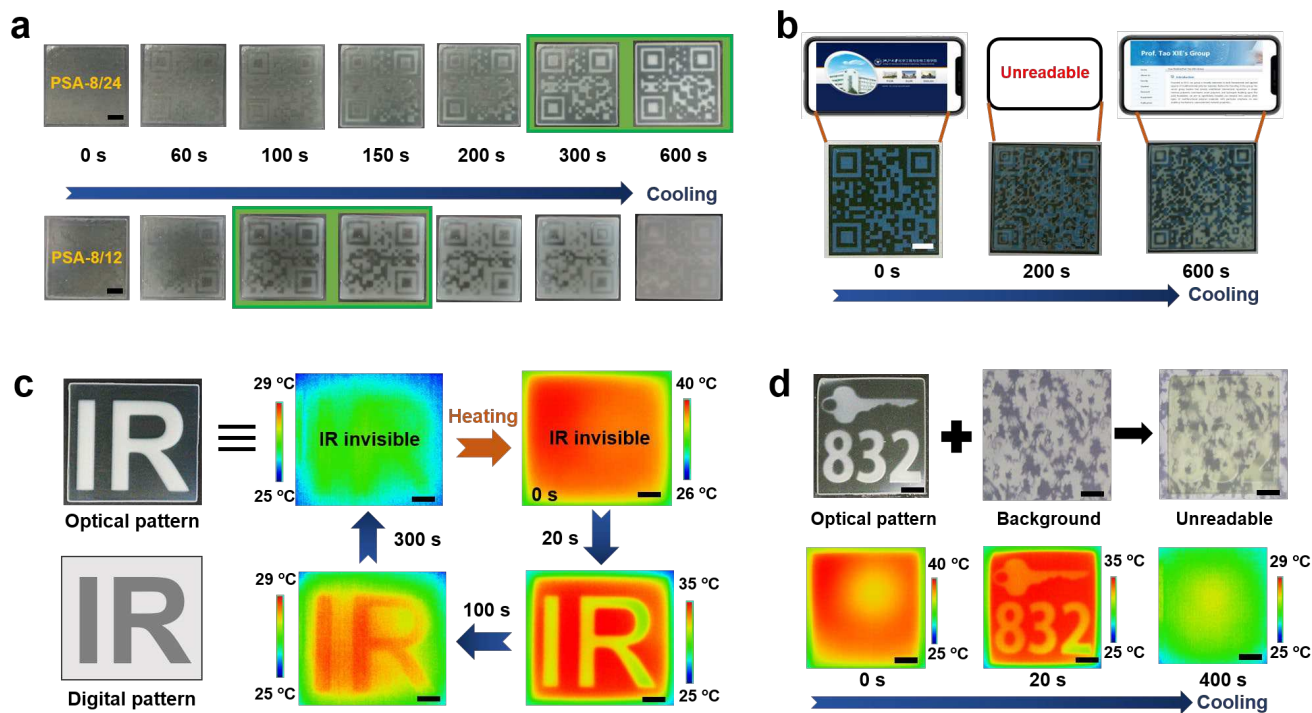
Fig. 3 Temporal evolution of optical and infrared images. a. Temporally programmed optical QR codes, with the green rectangular background indicating the readable ranges. **b.** Temporally switchable optical QR device using PSA-8/24. **c.** Temporal infrared evolution using PSA-8/30. **d.** Temporal infrared detection of an optical hidden information using PSA-12/30. All scale bars are 1 cm.
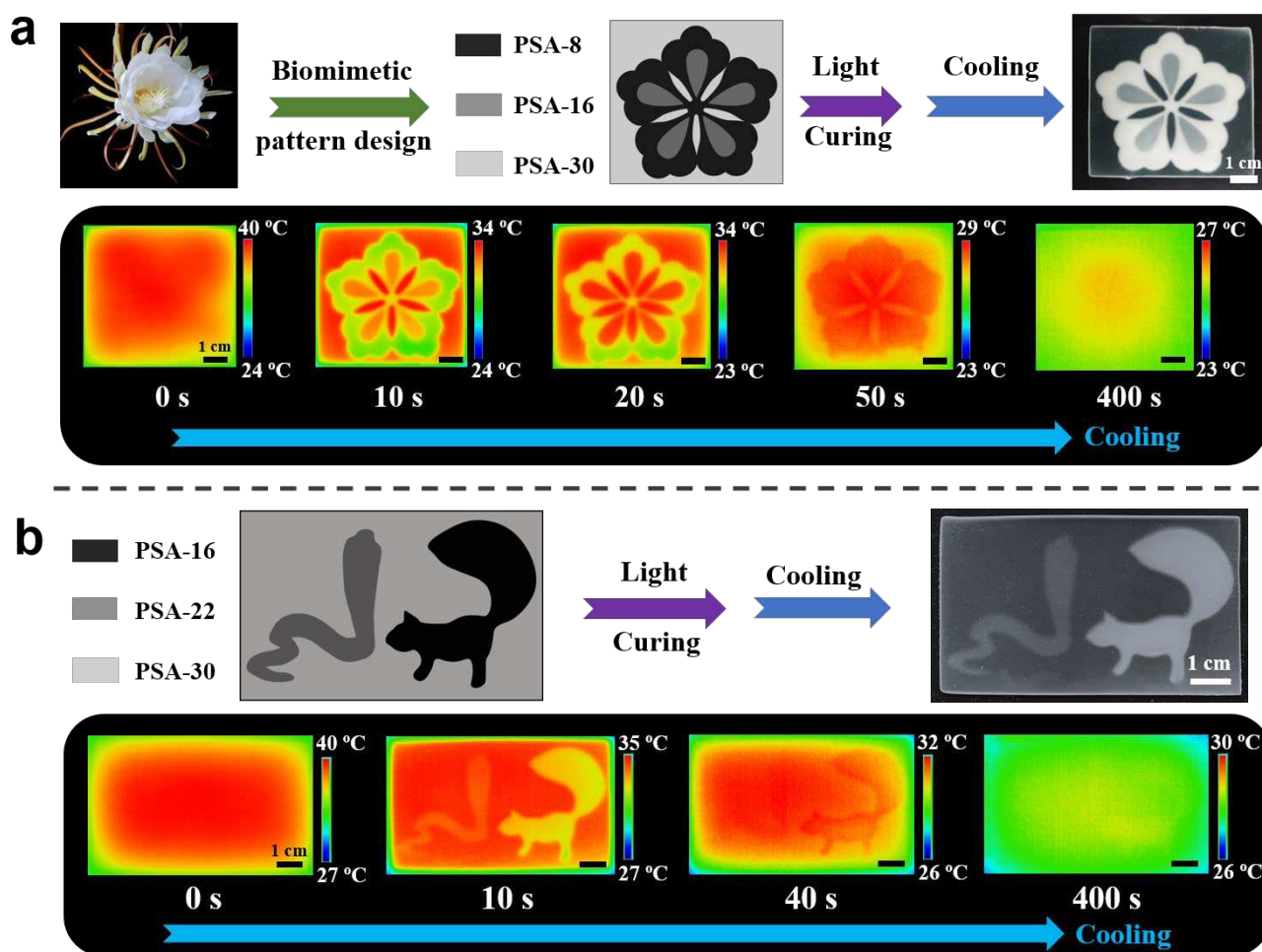
Fig. 4. Demonstrations of multi-temporal infrared information. a. Design and temporal infrared evolution of an epiphyllum pattern. **b.** Design and temporal infrared evolution of a squirrel-snake combination pattern.
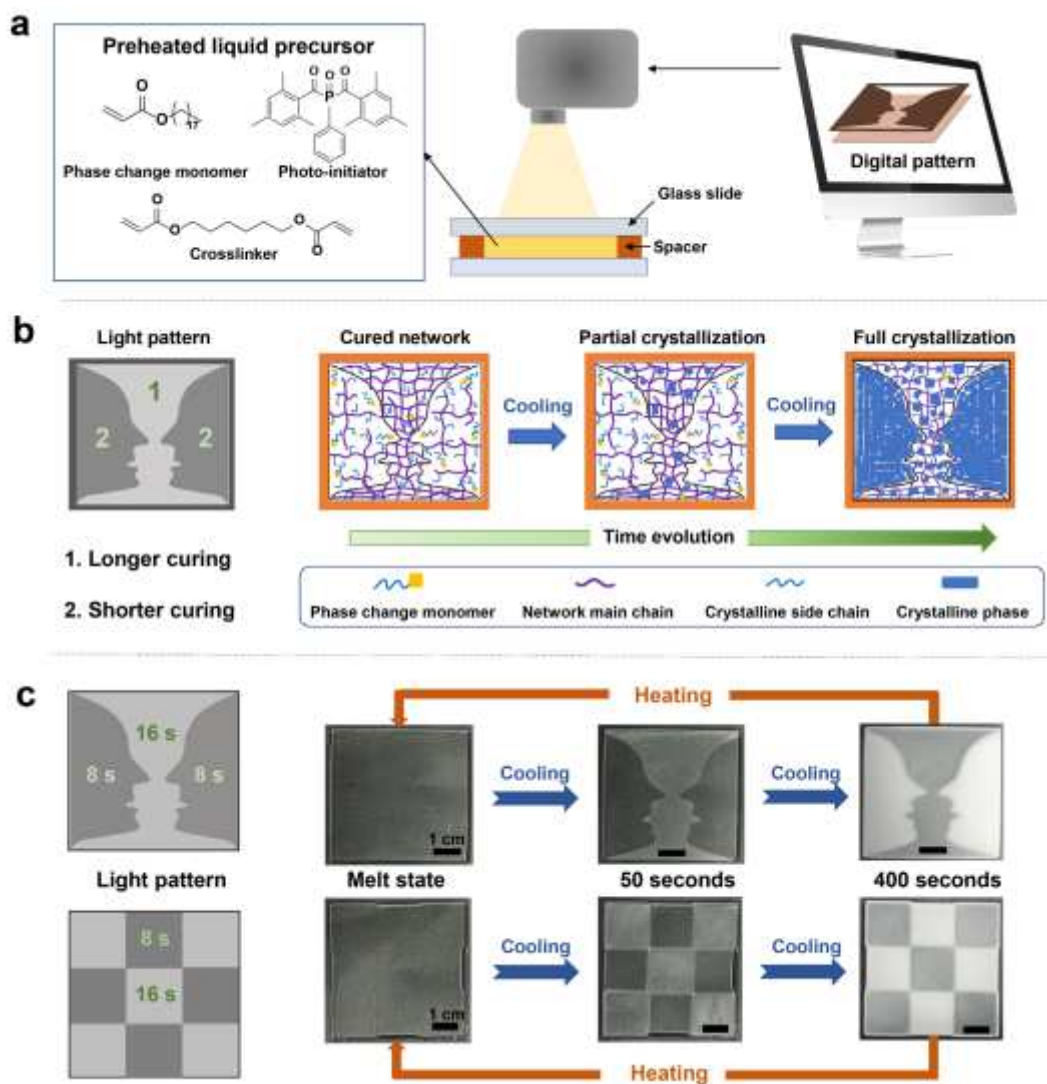
Figures

Figure 1

Materials, fabrication, and operating principle of the digital programmable phase change material. a. Precursors and digital curing setup. b. Light controlled network formation and crystallization. c. Reversal of the optical contrast for two digital cured patterns.
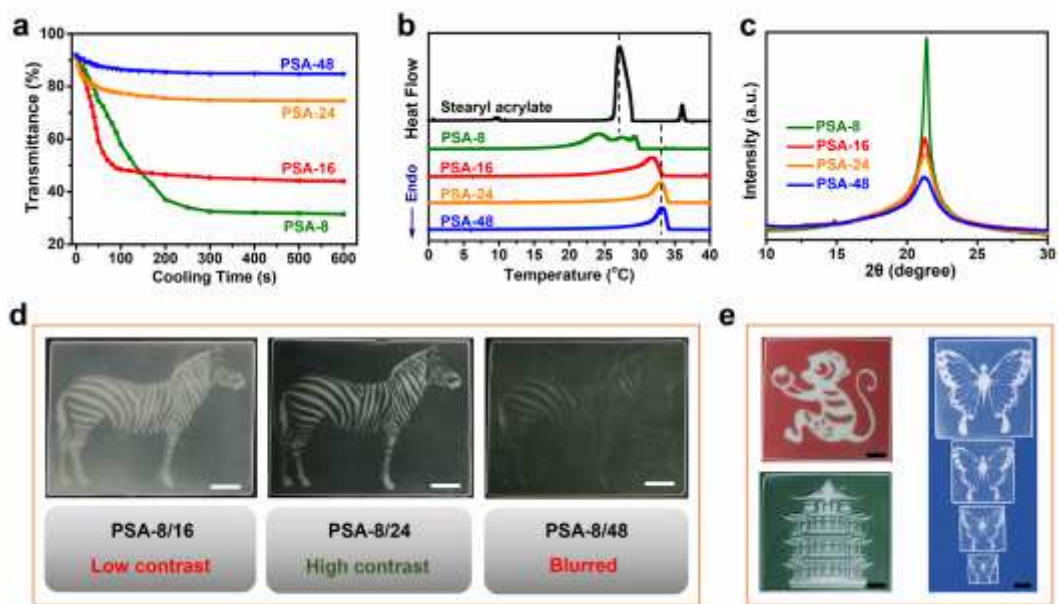
Figure 2

Crystallization behaviors of digitally cured phase change material and the optical contrast optimization. a. Time evolution of visible light transmittance upon cooling. b. Differential scanning calorimetry (DSC) crystallization curves. c. XRD patterns. d. Comparison of the optical contrast for the patterned samples with different curing time combinations. e. Diverse optical patterns with colored backgrounds obtained with a PSA-8/24 combination.
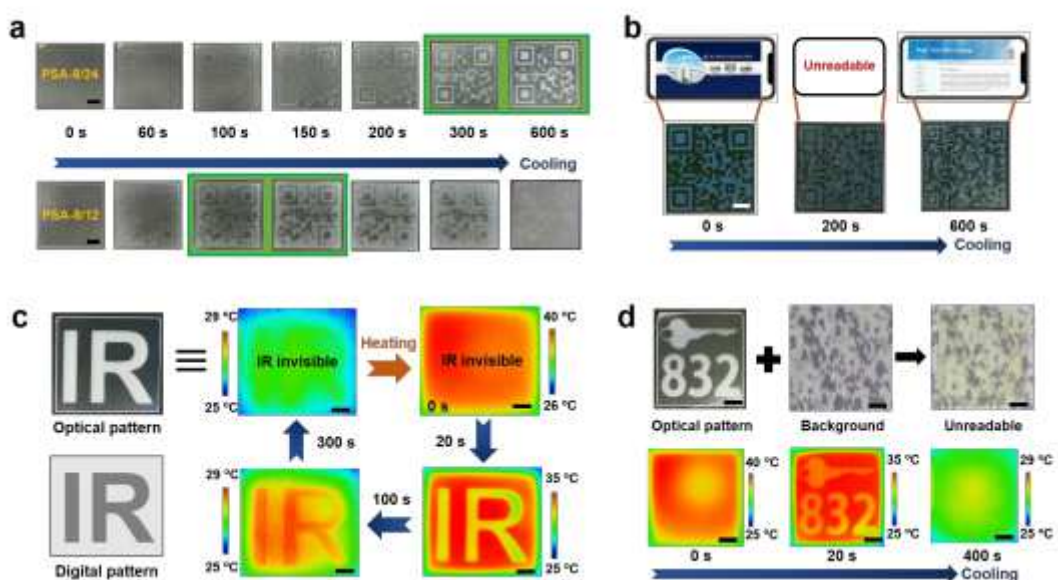

Figure 3

Temporal evolution of optical and infrared images. a. Temporally programmed optical QR codes, with the green rectangular background indicating the readable ranges. b. Temporally switchable optical QR device

using PSA-8/24. c. Temporal infrared evolution using PSA-8/30. d. Temporal infrared detection of an optical hidden information using PSA-12/30. All scale bars are 1 cm.
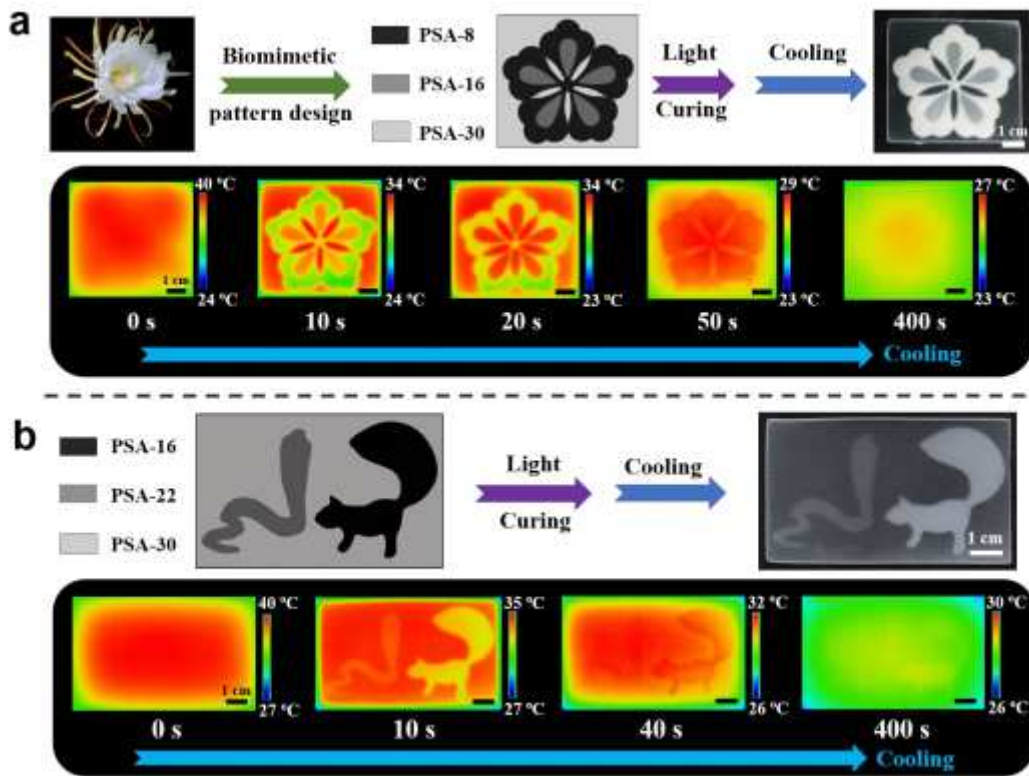

Figure 4

Demonstrations of multi-temporal infrared information. a. Design and temporal infrared evolution of an epiphyllum pattern. b. Design and temporal infrared evolution of a squirrel-snake combination pattern.

Supplementary Files

This is a list of supplementary files associated with this preprint. Click to download.

- supplementaryvideos.zip
- Supportinginfo.pdf